

Theory and Experiment for Flutter of a Rectangular Plate with a Fixed Leading Edge in Three-Dimensional Axial Flow

Samuel Chad Gibbs IV
9/28/2011
Advisor: Dr. Earl Dowell



Introduction

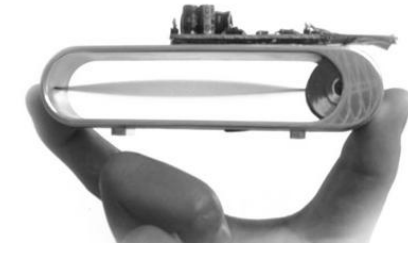


Problem Description

Further the understanding of dynamic instabilities in low aspect ratio cantilevered plates. Such systems exhibit limit cycle oscillations (LCO) that persist even if the free stream velocity falls below the flutter onset velocity

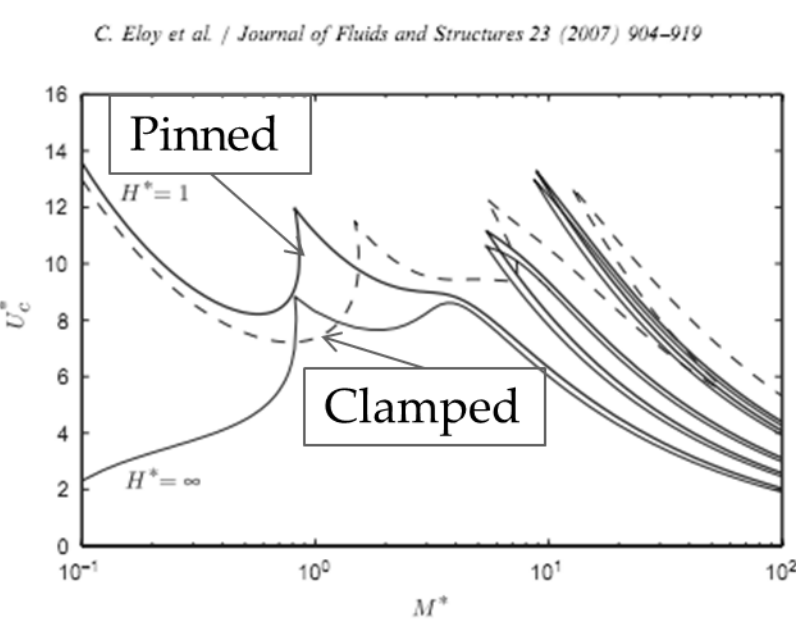
Motivation

- Energy harvesting from flutter
- Flutter prediction for Airplane control surfaces including noise suppression for landing aircraft (ongoing NASA research)



Previous Work

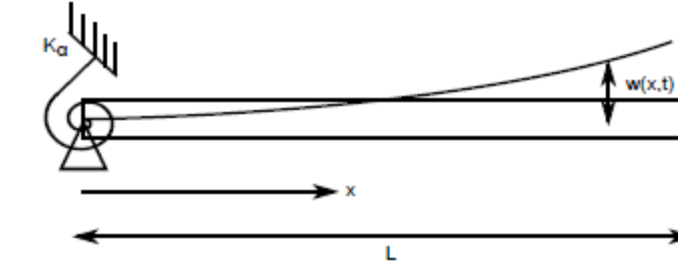
Previous work can be split into classical Theodorsen analysis with no wake in 2 and 3 dimensions, and full 2 dimension CFD solutions. In particular parameter studies for the flutter boundary and frequency have been conducted by Eloy et al. [1] to show that the flutter boundary is governed by the *aspect-ratio*, *mass ratio* and *boundary conditions*. The work of Eloy et al. [1] attempts a direct solution of the potential flow equations.



Research Methodology

A modification of an existing panel method used to model the aerodynamics for specific parameters was used. The vortex lattice model allows for the modeling of the wake left behind by the oscillating structure. This was coupled with a non-dimensional structural model derived using energy methods. The aeroelastic model was solved for a varying parameters, specifically the mass ratio, to determine to flutter boundary in parameter space. Further study was conducted on a model which included a leading edge torsional spring to model a transition in boundary conditions between pinned and clamped.

Single-Direction Structural Model



The first structural model which was used only allowed the plate displacement to vary as a function of its chord location(x) and time(t). First the natural modes and frequencies of the clamped-free and pinned-free boundary conditions were solved for using the equations of motion and natural boundary conditions derived from Hamilton's principal.

Table 1: Non-Dimensional Natural Frequencies

Mode Number	Pinned-Free Frequency	Clamped-Free Frequency
1	0	$(.517)^2 \pi^2$
2	$(2 - \frac{1}{2})^2 \pi^2$	$(1.49)^2 \pi^2$
3	$(3 - \frac{1}{2})^2 \pi^2$	$(2 - \frac{1}{2})^2 \pi^2$
...
n	$(n - \frac{1}{2})^2 \pi^2$	$(n - \frac{1}{2})^2 \pi^2$

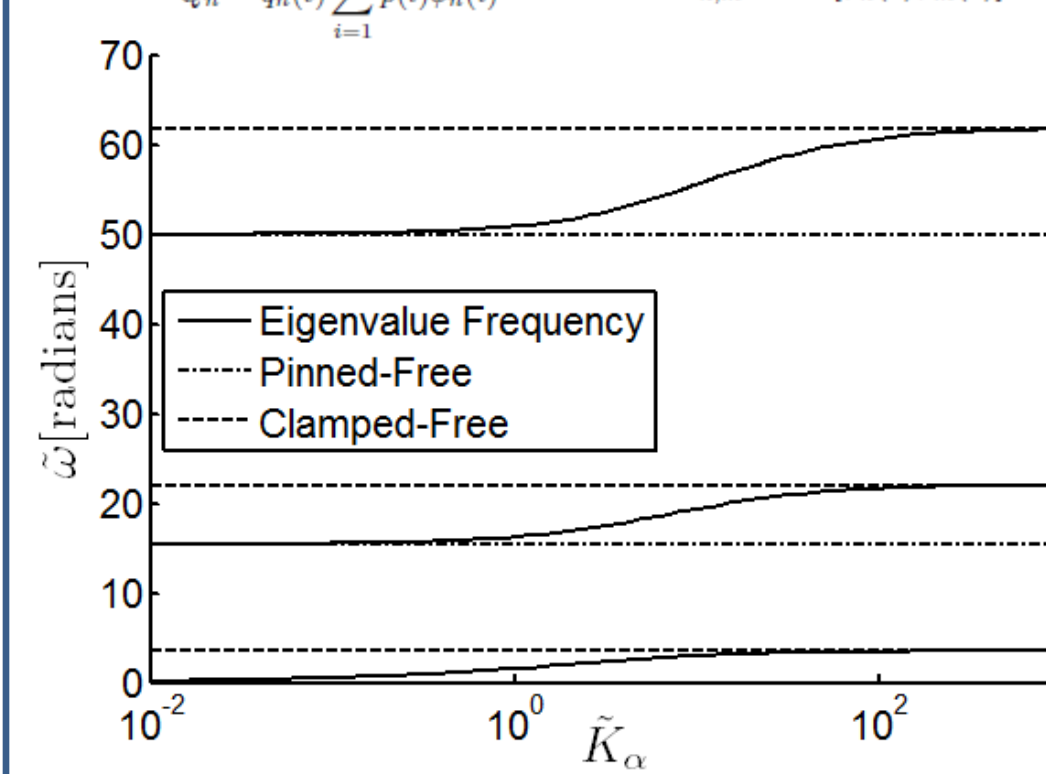
These structural modes and frequencies were then used as the assumed modes in the future aeroelastic and elastic simulations. In addition to the simple boundary conditions was the inclusion of a torsional spring at the simply supported end. The spring was modeled by adding the torsional spring energy to the potential energy expression and then using Lagrange's equation.

$$M\ddot{q} + (K + K_s)q = Q$$

$$\int_0^L m \delta w_n(x) \delta w_n(x) dx = \begin{cases} 0 & \text{for } n \neq k \\ M_n = \int_0^L m \delta w_n^2(x) dx & \text{for } n = k \end{cases}$$

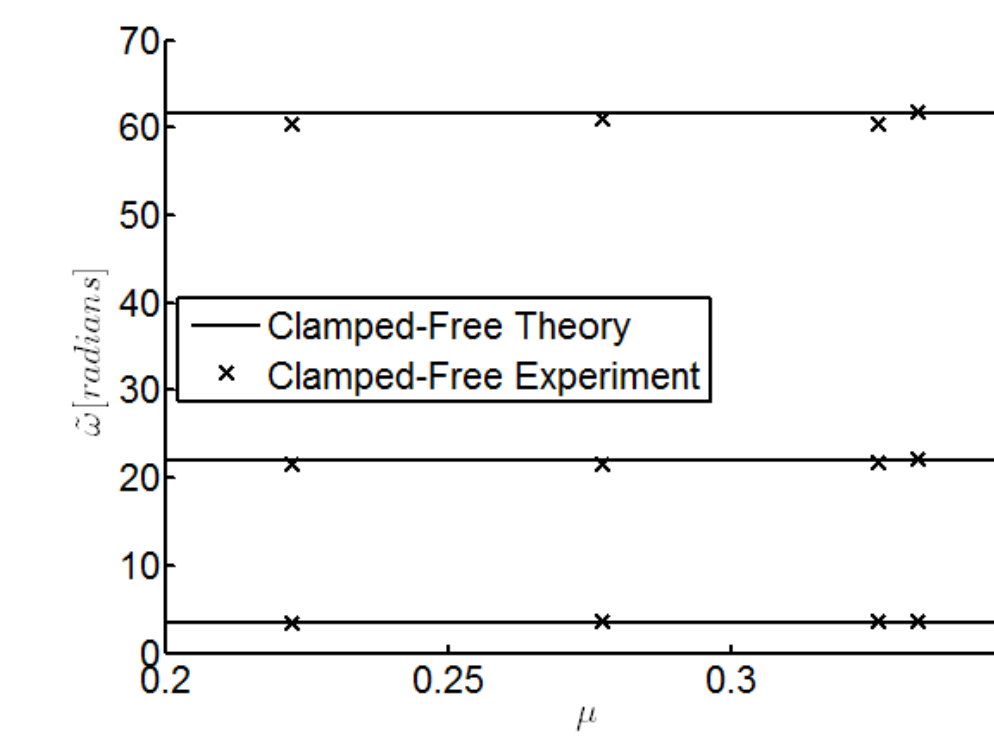
$$\int_0^L EI \delta w_n''(x) \delta w_n''(x) dx = \begin{cases} 0 & \text{for } n \neq k \\ K_n = \int_0^L EI \delta w_n''^2(x) dx & \text{for } n = k \end{cases}$$

$$Q_n = q_n(t) \sum_{j=1}^N \tilde{p}_j(t) \delta w_n(t) \quad K_{s,n,m} = K_s \delta_{n,m} \delta w_n(0)$$



Structural Experimental Results

Finally the structural simulations were compared to experimental results with good agreement suggesting that the model successfully captures the dynamics



Structural Model

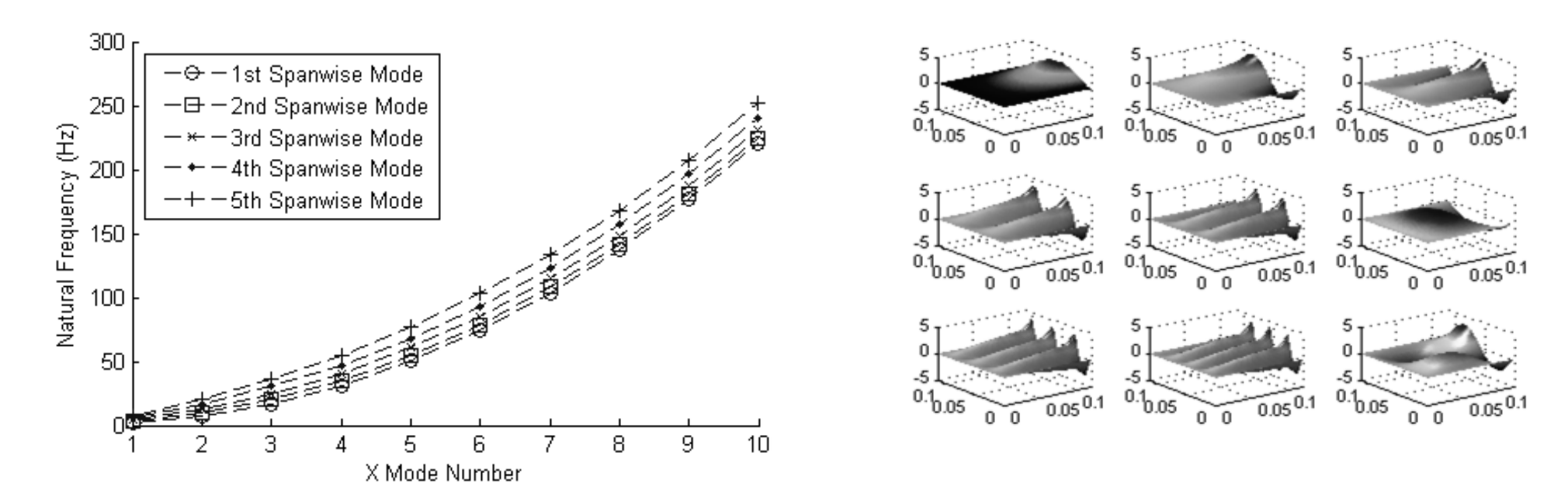
Multi-Directional Structural Model

When dealing with aspect ratios near one structural simulations suggested that there could be structural motion in both directions. To create the equations of motion the following modal expansion was assumed:

$$w(x, y, t) = \sum_{j,k} q_{jk}(t) \Psi_{jk}(x, y) \quad \Psi_{jk}(x, y) = \phi_j(x) \theta_k(y)$$

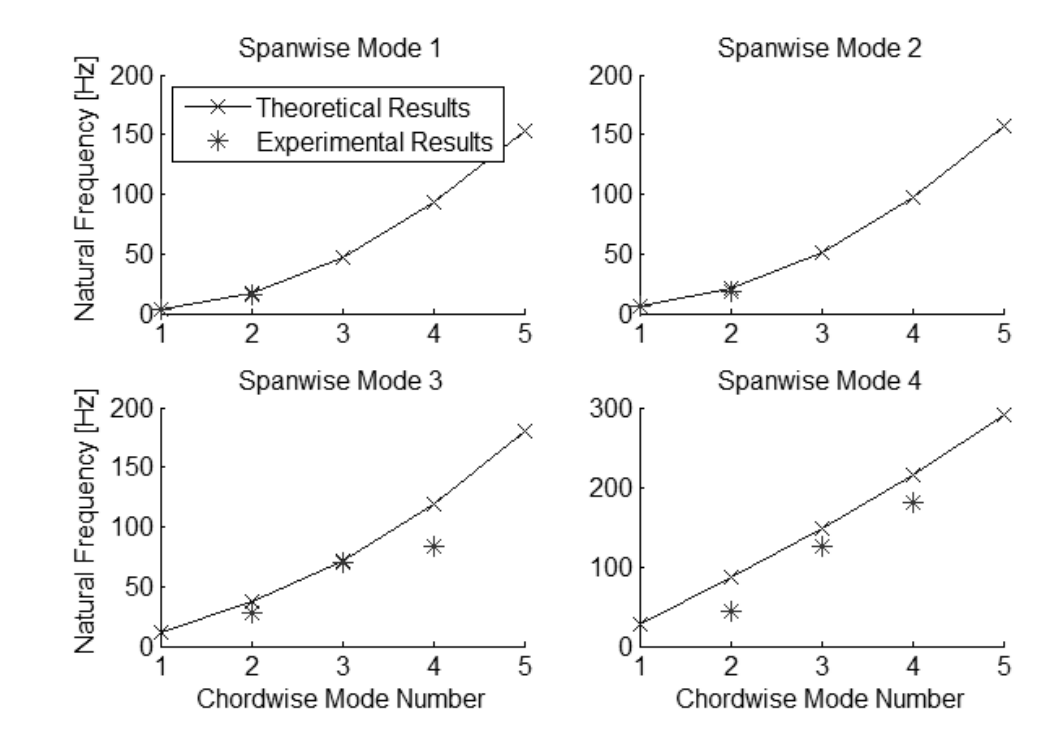
The equations show that the displacement is now assumed to vary in both the x and y directions and with time. The assumed structural mode shapes in the two directions are the single-direction mode shapes that satisfy the boundary conditions in that direction. As before the energies of the system were modeled and the equations were determined by applying Lagrange's equation.

Solving for the natural frequencies and mode shapes of the system yields the following figures.

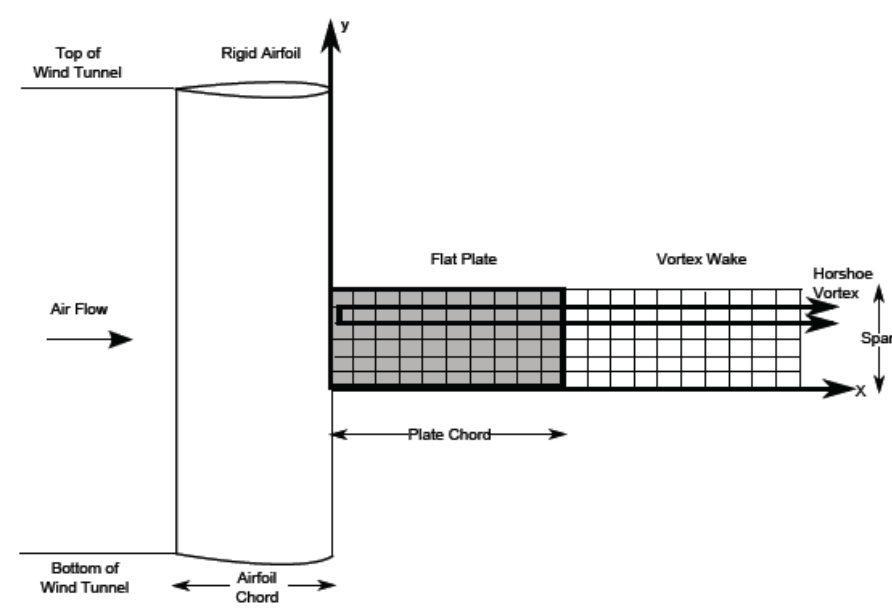


Structural Experimental Results

Structural simulations using the new model were conducted on an aspect ratio 1 plate made from an elastic material. The figure shows good agreement in magnitude and trend between the theory and experiment.

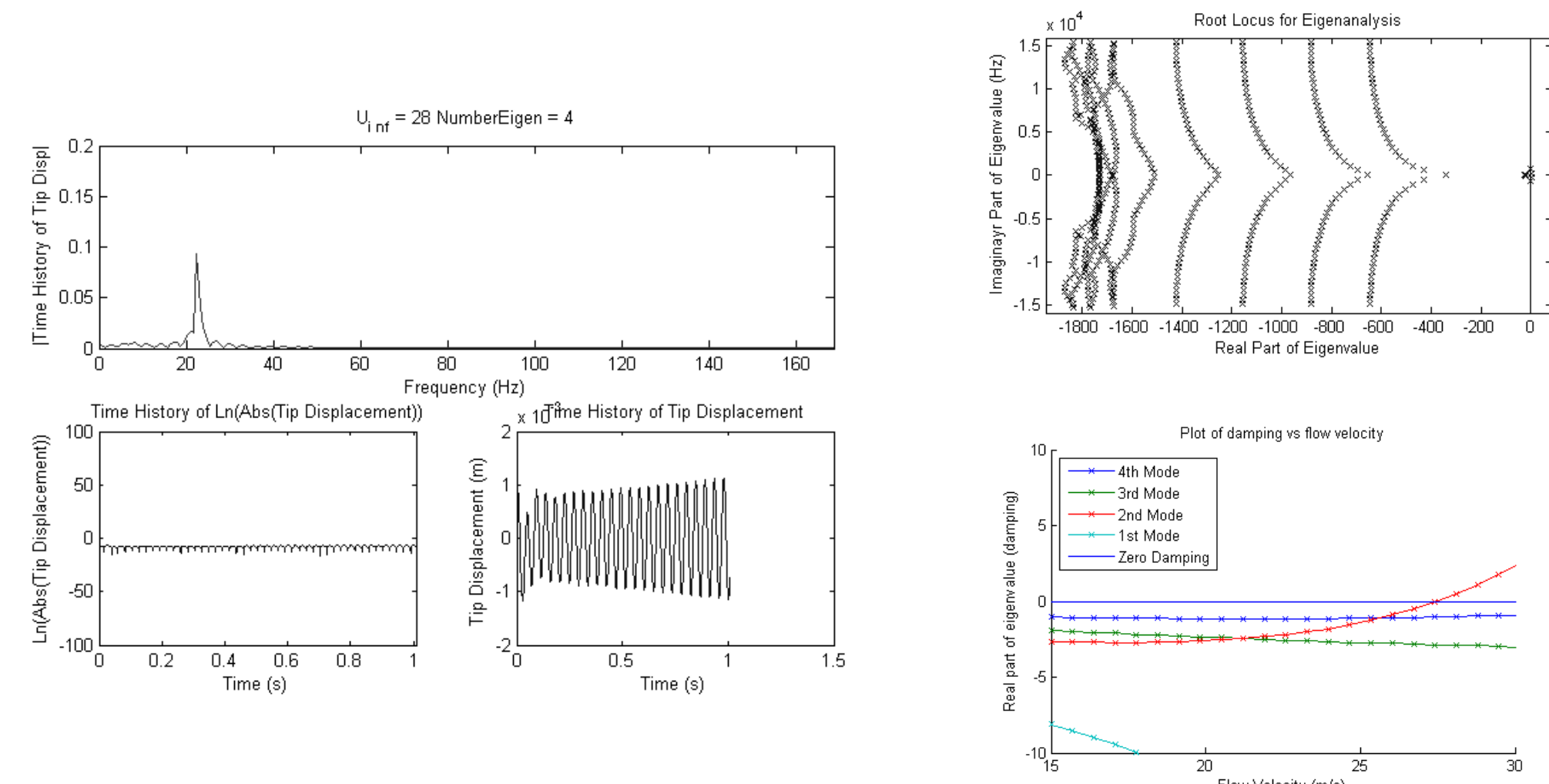


Vortex Lattice Method

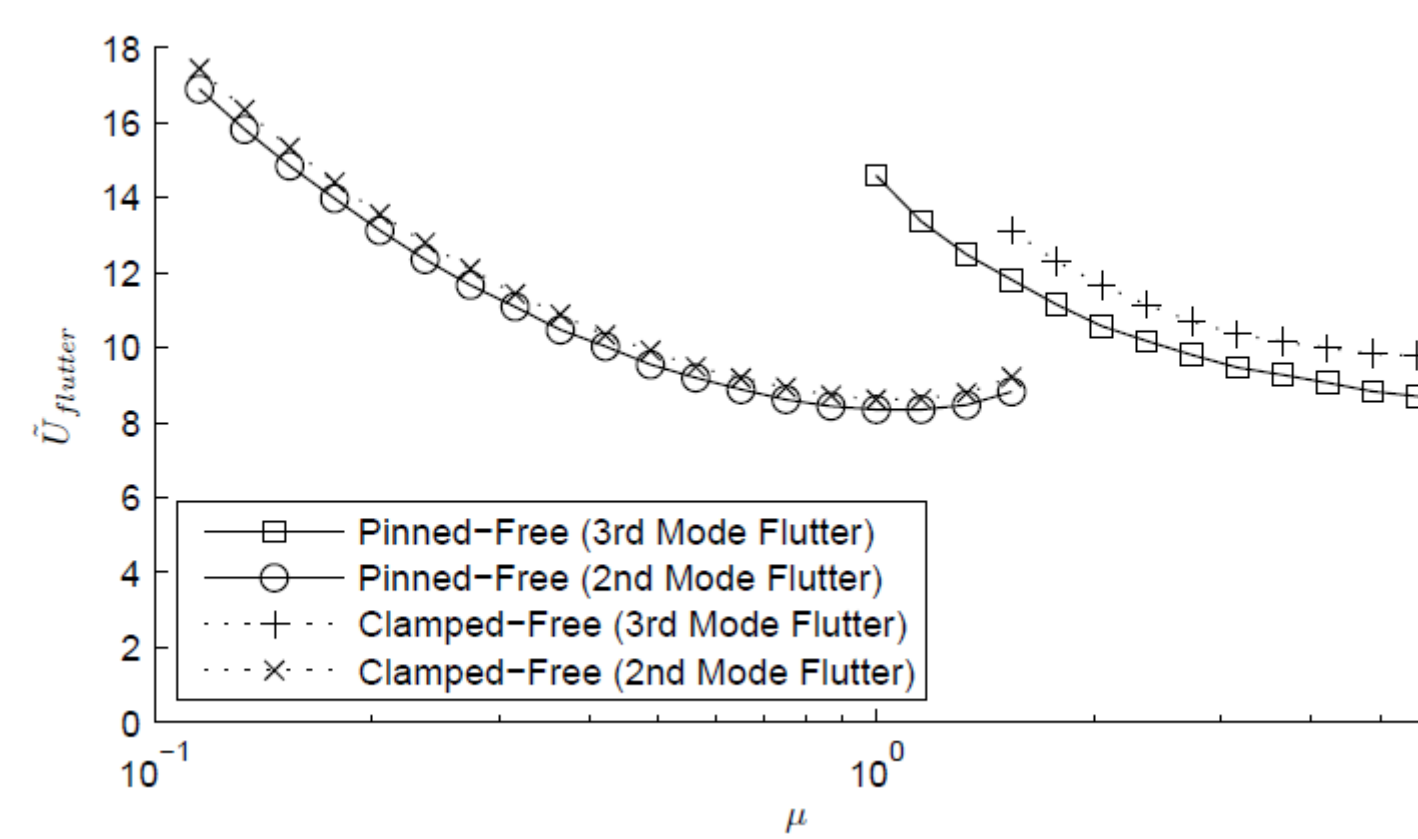


In order to solve for the stability of the aeroelastic system a method of modeling the aerodynamics must be implemented. For this research a linear *Vortex Lattice Method (VLM)* was used to model the aerodynamics. The method tracks the progression of finite number of horseshoe vortices. By knowing the strength or the vortices on the structure the forces on the structure can be calculated.

Once the aerodynamic forces have been determined the aeroelastic system must be solved. This can be done using a time simulation, shown on the left, or using an eigenvalue approach. The image in the bottom right is the visualization of all of the eigenvalues determined by a single simulation.



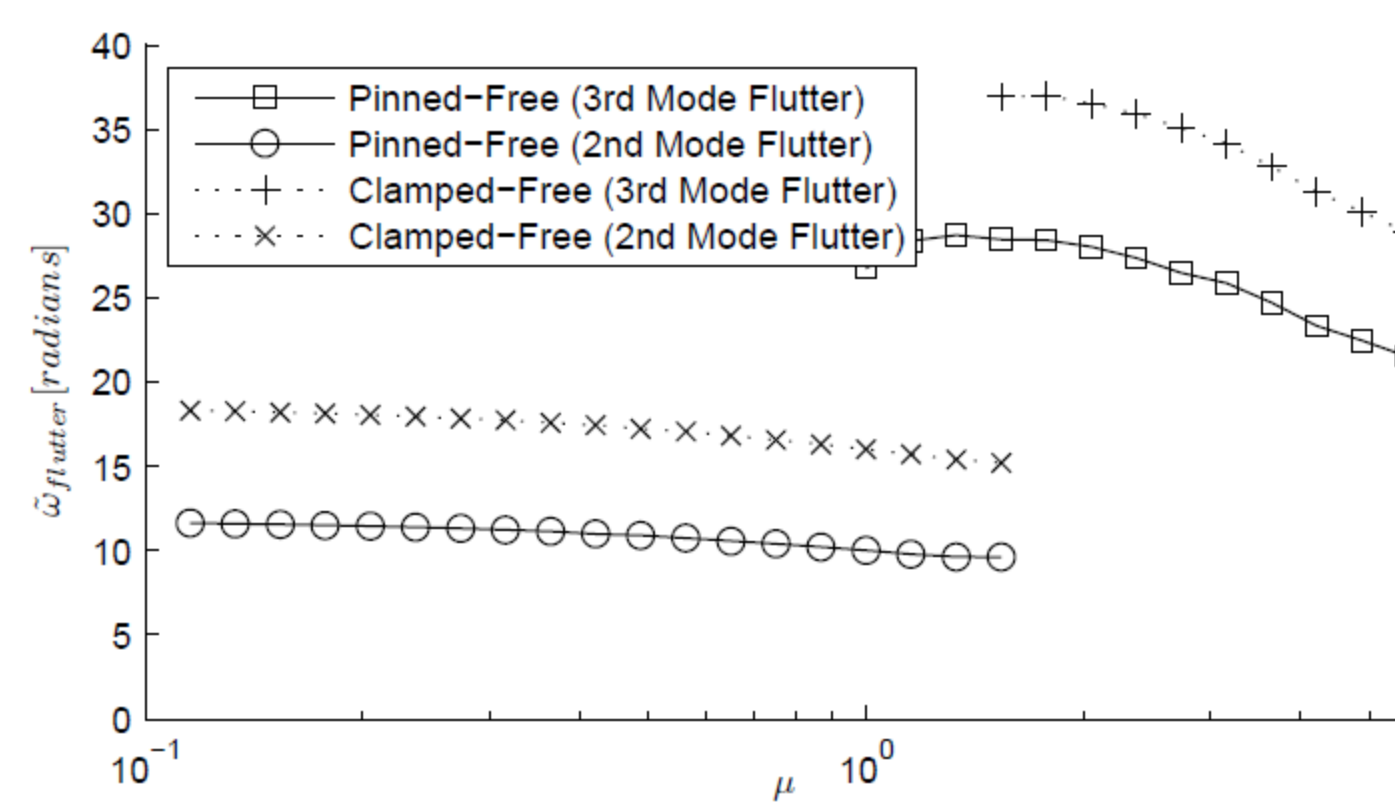
Aeroelastic Model



Parameter Variation Results

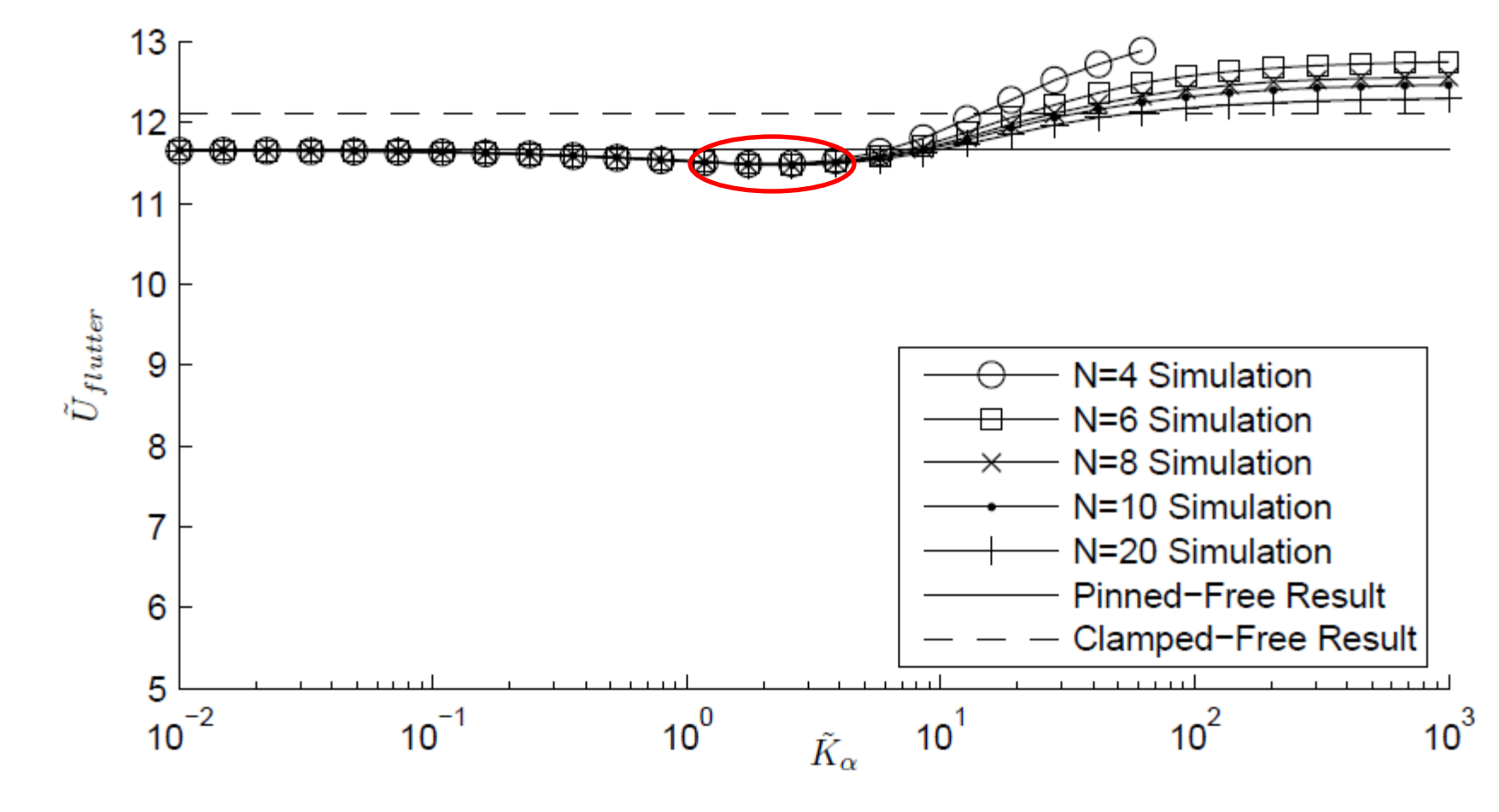
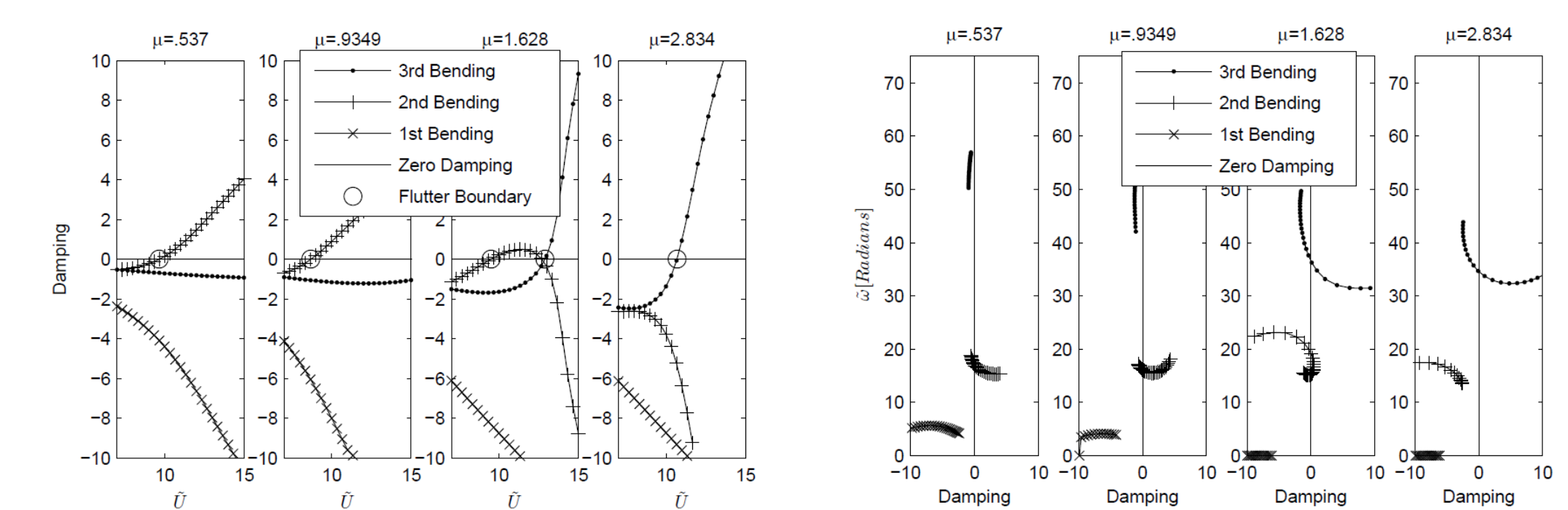
The goal of this aeroelastic analysis was to predict the flutter boundary in parameter space for the aeroelastic system for both pinned-free and clamped-free beams as well as the transition between the two modeled with the leading edge spring.

To the right, the leading edge spring flutter boundary is shown. Surprisingly there is a minimum flutter velocity that is not at either of the extrema of boundary conditions.



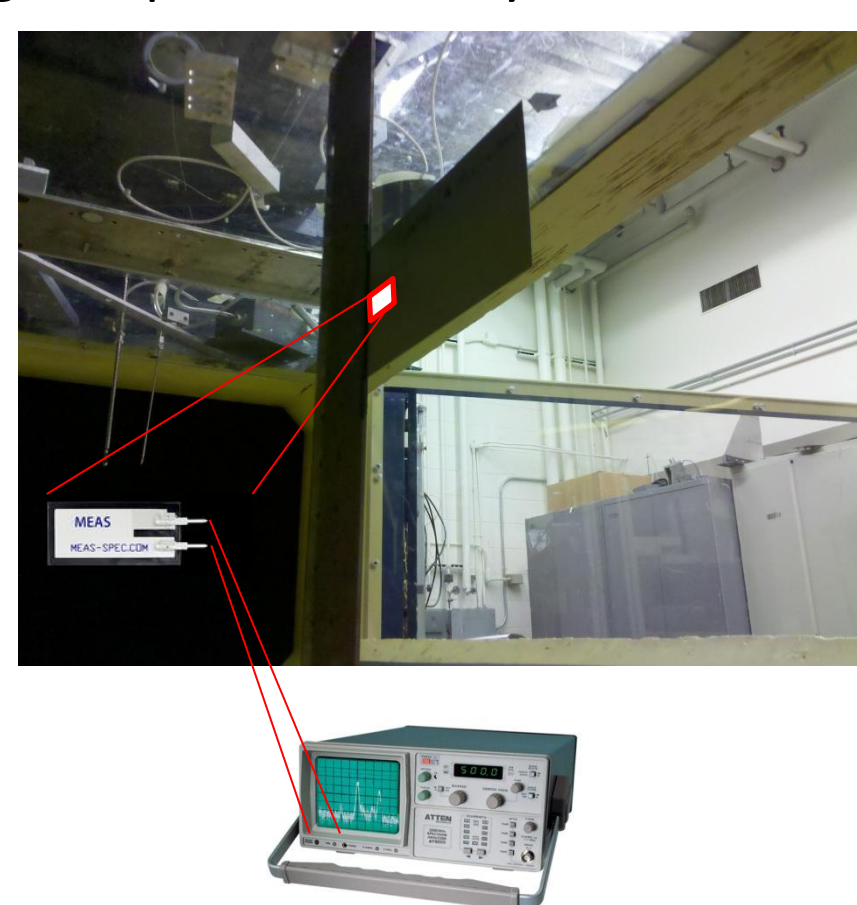
Mass Ratio Flutter Behavior Transition

Looking at the flutter boundary as a function of mass ratio shows an interesting behavior near a mass ratio of one as the flutter velocity for both boundary conditions jumps and the dominating flutter modes moves to a higher mode number. The two figures below capture the range of mass ratios over which this transition takes place for the clamped-free beam.



Experimental Setup

The table and figure below show the experimental setup including the test piece material as well as the measurement devices. Wind tunnel testing was completed in the Duke wind tunnel. The velocity and frequency at which the system enters a large amplitude limit cycle oscillation.



Property	Symbol	Value
Elastic plate properties		
Alloy		3003
Thickness	h	.381 mm, .25 mm and .13 mm
Density	ρ_s	2840 kg/m ³
Young's Modulus	E	72 GPa
Airfoil Chord		
Airfoil Chord		101 mm
Airfoil Span		550 mm
Air Density	ρ_a	1.2 kg/m ³
Piezoelectric Patch Properties		
Source		Measurement Specialty
Series		DT Series Patch
Size		30mm by 12mm
Spectrum Analyzer Properties		
Manufacturer		Scientific Atlanta
Name		Spectral Dynamics SD380

Discussion

For both the flutter velocity and the flutter frequency there was good agreement in both quantity and trend between the theory and experiment.

Future work is planned both theoretically and experimentally. Theoretically a wider range of boundary conditions in both directions will be modeled. Experimentally a larger range of mass ratios, including mass ratios where there is a transition between flutter mode should be attempted.

	Velocity	Frequency
Error	5.35%	-2.97%
Error Standard Deviation	1.65%	.89%
Max Error	6.87%	-3.54%

